

An Over-Massive Black Hole in a Typical Star-Forming Galaxy, 2 Billion Years After the Big Bang

Benny Trakhtenbrot,^{1*} C. Megan Urry,^{2,3,4} Francesca Civano,^{3,5}
David J. Rosario,⁶ Martin Elvis,⁵ Kevin Schawinski,¹
Hyewon Suh,^{5,7} Angela Bongiorno,⁸ Brooke D. Simmons⁹

¹Department of Physics, Institute for Astronomy, ETH Zurich,
Wolfgang-Pauli-Strasse 27, Zurich 8093, Switzerland

²Department of Physics, Yale University, PO Box 208120, New Haven, CT 06520-8120, USA

³Yale Center for Astronomy and Astrophysics, 260 Whitney ave., New Haven, CT 06520-8121, USA

⁴Department of Astronomy, Yale University, PO Box 208101, New Haven, CT 06520-8101, USA

⁵Harvard-Smithsonian Center for Astrophysics, 60 Garden st., Cambridge, MA 02138, USA

⁶Max-Planck-Institut für Extraterrestrische Physik (MPE), Postfach 1312, 85741 Garching, Germany

⁷Institute for Astronomy, University of Hawaii, 2680 Woodlawn Drive, Honolulu, HI 96822, USA

⁸INAF-Osservatorio Astronomico di Roma, Via di Frascati 33, I-00040 Monteporzio Catone, Rome, Italy

⁹Oxford Astrophysics, Denys Wilkinson Building, Keble Road, Oxford OX1 3RH, UK

*Corresponding author. E-mail: benny.trakhtenbrot@phys.ethz.ch

Supermassive black holes (SMBHs) and their host galaxies are generally thought to coevolve, so that the SMBH achieves up to about 0.2 to 0.5% of the host galaxy mass in the present day. The radiation emitted from the growing SMBH is expected to affect star formation throughout the host galaxy. The relevance of this scenario at early cosmic epochs is not yet established. We present spectroscopic observations of a galaxy at redshift $z = 3.328$, which hosts an actively

accreting, extremely massive BH, in its final stages of growth. The SMBH mass is roughly one-tenth the mass of the entire host galaxy, suggesting that it has grown much more efficiently than the host, contrary to models of synchronized coevolution. The host galaxy is forming stars at an intense rate, despite the presence of a SMBH-driven gas outflow.

Several lines of observational evidence, spanning a wide range of cosmic epochs, have led to a commonly accepted picture wherein supermassive black holes (SMBHs, $M_{\text{BH}} > 10^6 M_{\odot}$; M_{\odot} is the solar mass) coevolve with their host galaxies (1–4). Moreover, energy- and/or momentum-driven “feedback” from accreting SMBHs (Active Galactic Nuclei; AGN) is thought to quench star formation in the host galaxy (5). To directly test the relevance of such scenarios at early cosmic epochs (high redshifts, z) requires the most basic properties of SMBHs and their hosts, including masses and growth rates, to be observed. Several observational studies found that at $z \lesssim 2$ (more than 3.3 billion years after the Big Bang), the typical BH-to-stellar mass ratio, M_{BH}/M_* , increases towards higher redshifts (6–8), suggesting that some SMBHs were able to gather mass more efficiently, or faster, than the stellar populations in their hosts. To date, measurements of M_{BH} at earlier epochs ($z > 2$) have only been conducted for small samples of extremely luminous objects [$L_{\text{AGN}} > 10^{46} \text{ erg s}^{-1}$ (9–12)] representing a rare subset of all accreting SMBHs, with number densities of order 1 to 10 per Gpc^3 [i.e., $\sim 10^{-9}$ to 10^{-8} Mpc^{-3} (13)]. Moreover, the high AGN luminosities in such sources overwhelm the host galaxy emission and prohibit a reliable determination of M_* , and therefore of M_{BH}/M_* . We initiated an observational campaign aimed at estimating M_{BH} in x-ray–selected, unobscured $z \sim 3$ to 4 AGN within the Cosmic Evolution Survey field [COSMOS; (14)]. Such sources have lower AGN luminosities and are more abundant than the aforementioned luminous sources by factors of 100 to 1000 (13, 15) and thus form a more representative subset of the general AGN population. Moreover, the fainter AGN luminosities and rich multiwavelength coverage of AGN

within the COSMOS field enable reliable measurements of the mass and growth rate of the stellar populations in the host galaxies (M_* and star-formation rate, SFR).

CID-947 is an x-ray-selected, unobscured AGN at $z = 3.328$, detected in both *XMM-Newton* and *Chandra* x-ray imaging data of the COSMOS field [see Fig. S4 and sections S2 and S4 in the supplementary materials (16)]. We obtained a near-infrared (IR) *K*-band spectrum of CID-947 using the MOSFIRE instrument at the W. M. Keck telescope, which at $z = 3.328$ covers the hydrogen $H\beta$ broad emission line (see details in section S1 in the supplementary materials). The calibrated spectrum shows a very broad $H\beta$ emission line, among other features (Fig. 1). Our spectral analysis indicates that the monochromatic AGN luminosity at rest-frame 5100 Å is $L_{5100} = 3.58^{+0.07}_{-0.08} \times 10^{45} \text{ erg s}^{-1}$. The typical line-of-sight velocity, i.e. the full-width at half-maximum of the line, is $11330^{+800}_{-870} \text{ km s}^{-1}$ (see section S1.2 in the supplementary materials). By combining this line width with the observed L_{5100} and relying on an empirically calibrated estimator for M_{BH} , based on the virial motion of ionized gas near the SMBH (17), we obtain $M_{\text{BH}} = 6.9^{+0.8}_{-1.2} \times 10^9 M_{\odot}$. All the reported measurement-related uncertainties are derived by a series of simulations and represent the 16th and 84th quantiles of the resulting distributions. These simulations indicate a SMBH mass larger than $3.6 \times 10^9 M_{\odot}$ at the 99% confidence level (see sections S1.2 and S3 for more details). Determinations of M_{BH} from single-epoch spectra of the $H\beta$ emission line are known to also be affected by significant systematic uncertainties, of up to ~ 0.3 to 0.4 dex. For a detailed discussion of some of the systematics and related issues, see §S3 in the supplementary materials. This high M_{BH} is comparable with some of the most massive BHs known to date in the local universe (18), or with the masses of the biggest BHs in the much rarer, more luminous AGN at $z \sim 2$ to 4 [e.g., (9)]. The bolometric luminosity of CID-947 is in the range $L_{\text{bol}} \simeq (1.1 - 2.2) \times 10^{46} \text{ erg s}^{-1}$, estimated either from the observed optical luminosity or the multiwavelength spectral energy distribution. Combined with the measured

M_{BH} , we derive a normalized accretion rate of $L/L_{\text{Edd}} \simeq 0.01$ to 0.02 . This value is lower, by at least an order of magnitude, than the accretion rates of known SMBHs at $z \sim 3.5$ [e.g., (9, 10)]. Further assuming a standard radiative efficiency of 10%, we obtain an e -folding time scale for the SMBH mass of at least 2.1×10^9 (Gy; see section S3), which is longer than the age of the universe at $z = 3.328$. By contrast, even the most extreme models for the emergence of “seed” BHs predict masses no larger than $M_{\text{seed}} \sim 10^6 M_{\odot}$ at $z \sim 10$ to 20 [e.g., (19)]. Therefore, the SMBH powering CID–947 had to grow at much higher accretion rates and at a high duty cycle in the past, to account for the high observed M_{BH} only 1.7 Gyr after $z \simeq 20$. CID–947 could have evolved from a parent population similar to the fast-growing SMBHs observed in $z \gtrsim 5$ quasars, which have $L/L_{\text{Edd}} \sim 0.5$ to 1 and $M_{\text{BH}} \simeq 10^9 M_{\odot}$ [e.g., (11, 12)]. The requirement for a high accretion rate in the very recent past is supported by the clear presence of a high-velocity outflow of ionized gas, observed in the rest-frame ultraviolet spectrum of the source (fig. S4). The broad absorption features of C IV $\lambda 1549$ and Si IV $\lambda 1400$ have maximal velocities of $v_{\text{max}} \simeq 12,000 \text{ km s}^{-1}$. Assuming that this outflow is driven by radiation pressure, these velocities require accretion rates of $L/L_{\text{Edd}} \gtrsim 0.1$, as recently as 10^5 to 10^6 years before the observed epoch (see section S4). We conclude that the SMBH powering CID–947 is in the final stages of growth and that we are witnessing the shut-down of accretion onto one of the most massive BHs known to date.

The rich collection of ancillary COSMOS multiwavelength data available for CID–947 enables us to study the basic properties of its host galaxy (see details in section S2 in the supplementary materials). A previously published analysis of the observed spectral energy distribution of the emission from the source reveals an appreciable stellar emission component, originating from $5.6_{-0.4}^{+2.8} \times 10^{10} M_{\odot}$ in stars (20). Our own analysis provides a yet lower stellar mass, of $M_{*} = 4.4_{-0.5}^{+0.4} \times 10^{10} M_{\odot}$. However, we focus on the previously determined, higher stellar mass, as a conservative estimate. The source is also detected at far-IR and (sub)millimeter

wavelengths, which allows us to constrain the SFR in the host galaxy to about $400 M_{\odot} \text{ year}^{-1}$. The stellar mass of the host galaxy is consistent with the typical value for star-forming galaxies at $z \sim 3$ to 4 [i.e., the “break” in the mass function of galaxies; (21)]. Similarly, the combination of M_* and SFR is consistent with the typical values observed at $z \sim 3$ to 4, which appear to follow the so-called main sequence of star-forming galaxies (22). Thus, the host galaxy of CID-947 is a typical star-forming galaxy for its redshift, representing a population with a number density of about $5 \times 10^{-5} \text{ Mpc}^{-3}$ [e.g., (21)]. This suggests that neither the intense, ionizing radiation that emerged during the fast SMBH growth, nor the AGN-driven outflow, have quenched star formation in the host galaxy. The relatively high stellar mass and SFR of the host galaxy further suggest that it is unlikely that the AGN affected the host in yet earlier epochs. That is, even in this case of extreme SMBH growth, there is no sign of AGN-driven suppression of star formation in the host.

Our analysis indicates that the BH-to-stellar mass ratio for CID-947 is $M_{\text{BH}}/M_* \simeq 1/8$. In comparison, most local (dormant) high-mass BHs typically have $M_{\text{BH}}/M_* \sim 1/700$ to $1/500$ [see Fig. 2 and, e.g., (4, 23)]. The M_{BH}/M_* value that we find for CID-947 is thus far higher than typically observed in high-mass systems in the local universe, by at least an order of magnitude and more probably by a factor of about 50. The only local system with a comparably extreme mass ratio is the galaxy NGC 1277, which was reported to have $M_{\text{BH}}/M_* \simeq 1/7$ [with $M_{\text{BH}} = 1.7 \times 10^{10} M_{\odot} \simeq 2.5 \times M_{\text{BH}}(\text{CID-947})$; see (24), but also (25)]. At earlier epochs (still $z < 2$), the general trend is for M_{BH}/M_* to increase slightly with redshift, but typically not beyond $M_{\text{BH}}/M_* \sim 1/100$ (see Fig. 3). Only a few systems with reliable estimates of M_{BH} show M_{BH}/M_* reaching as high as $1/30$ [e.g., (6–8)].

Given the high masses of both the SMBH and stellar population in CID-947, we expect this system to retain an extreme M_{BH}/M_* throughout its evolution, from $z = 3.328$ to the

present-day universe. Because the M_{BH} that we find is already comparable to the most massive BHs known, it is unlikely that the SMBH will experience any further appreciable growth (i.e., beyond $M_{\text{BH}} \simeq 10^{10} M_{\odot}$). Indeed, if the SMBH accretes at the observed rate through $z = 2$, it will reach the extreme value of $\sim 10^{10} M_{\odot}$, and by $z = 1$ it will have a final mass of $\sim 2.5 \times 10^{10} M_{\odot}$. As for the host galaxy, we can constrain its subsequent growth following several different assumptions. First, if one simply assumes that the galaxy will become as massive as the most massive galaxies in the local universe [$M_* \simeq 10^{12} M_{\odot}$; (26)], then the implied final mass ratio is on the order of $M_{\text{BH}}/M_* \sim 1/100$. Alternatively, we consider more realistic scenarios for the future growth of the stellar population, relying on the observed mass (M_*) and growth rate (SFR). Our calculations involve different scenarios for the decay of star formation in the galaxy (see section S5 in the supplementary materials), and predict final stellar masses in the range $M_*(z = 0) \simeq (2 - 7) \times 10^{11} M_{\odot}$, which is about an order of magnitude higher than the observed mass at $z = 3.328$. The inferred final mass ratio is $M_{\text{BH}}/M_* \sim 1/50$. This growth can only occur if star formation continues for a relatively long period ($\gtrsim 1$ Gy) and at a high rate ($> 50 M_{\odot} \text{ year}^{-1}$). This would require the presence of a substantial reservoir, or the accretion, of cold gas, which, however, could not increase the SMBH mass by much. Finally, in the most extreme scenario, the star formation shuts down almost immediately (i.e., due to the AGN-driven outflow), and the system remains “frozen” at $M_{\text{BH}}/M_* \sim 1/10$ throughout cosmic time. If the SMBH does indeed grow further (i.e., beyond $10^{10} M_{\odot}$), this would imply yet higher M_{BH}/M_* . Thus, the inferred final BH-to-stellar mass ratio for CID-947 is, in the most extreme scenarios, about $M_{\text{BH}}/M_* \sim 1/100$, and probably much higher (see Fig. 2).

CID-947 therefore represents a progenitor of the most extreme, high-mass systems in the local universe, like NGC 1277. Such systems are not detected in large numbers, perhaps due to observational selection biases. The above considerations indicate that the local relics of systems like CID-947 are galaxies with at least $M_* \sim 5 \times 10^{11} M_{\odot}$. Such systems are predominantly

quiescent (i.e., with low star-formation rates, $\text{SFR} \ll 1 M_{\odot} \text{ year}^{-1}$) and relatively rare in the local universe, with typical number densities on the order of $\sim 10^{-5} \text{ Mpc}^{-3}$ (26). We conclude that CID-947 provides direct evidence that at least some of the most massive BHs, with $M_{\text{BH}} \gtrsim 10^{10} M_{\odot}$, already in place just 2 Gy after the Big Bang, did not shut down star formation in their host galaxies. The host galaxies may experience appreciable mass growth in later epochs, without much further black hole growth, resulting in very high stellar masses but still relatively high M_{BH}/M_{*} . Lower-mass systems may follow markedly different coevolutionary paths. However, systems with M_{BH}/M_{*} as high as in CID-947 may be not as rare as previously thought, as they can be consistently observed among populations with number densities on the order of $\sim 10^{-5} \text{ Mpc}^{-3}$, both at $z > 3$ and in the local universe, and not just among the rarest, most luminous quasars.

References and Notes

1. L. Ferrarese, D. Merritt, *The Astrophysical Journal* **539**, L9 (2000).
2. K. Gebhardt, *et al.*, *The Astrophysical Journal* **539**, L13 (2000).
3. X. Z. Zheng, *et al.*, *The Astrophysical Journal* **707**, 1566 (2009).
4. J. Kormendy, L. C. Ho, *Annual Review of Astronomy and Astrophysics* **51**, 511 (2013).
5. A. C. Fabian, *Annual Review of Astronomy and Astrophysics* **50**, 455 (2012).
6. A. Merloni, *et al.*, *The Astrophysical Journal* **708**, 137 (2010).
7. R. Decarli, *et al.*, *Monthly Notices of the Royal Astronomical Society* **402**, 2453 (2010).
8. V. N. Bennert, M. W. Auger, T. Treu, J.-H. Woo, M. A. Malkan, *The Astrophysical Journal* **742**, 107 (2011).

9. O. Shemmer, *et al.*, *The Astrophysical Journal* **614**, 547 (2004).
10. H. Netzer, P. Lira, B. Trakhtenbrot, O. Shemmer, I. Cury, *The Astrophysical Journal* **671**, 1256 (2007).
11. G. De Rosa, *et al.*, *The Astrophysical Journal* **739**, 56 (2011).
12. B. Trakhtenbrot, H. Netzer, P. Lira, O. Shemmer, *The Astrophysical Journal* **730**, 7 (2011).
13. D. Masters, *et al.*, *The Astrophysical Journal* **755**, 169 (2012).
14. N. Z. Scoville, *et al.*, *The Astrophysical Journal Supplement Series* **172**, 1 (2007).
15. F. Civano, *et al.*, *The Astrophysical Journal* **741**, 91 (2011).
16. Data and methods, supplementary text, figures and tables are available as supplementary materials on Science Online.
17. Y. Shen, *Bulletin of the Astronomical Society of India* **41**, 61 (2013).
18. N. J. McConnell, *et al.*, *The Astrophysical Journal* **756**, 179 (2012).
19. M. Volonteri, *The Astronomy and Astrophysics Review* **18**, 279 (2010).
20. A. Bongiorno, *et al.*, *Monthly Notices of the Royal Astronomical Society* **427**, 3103 (2012).
21. O. Ilbert, *et al.*, *Astronomy and Astrophysics* **556**, A55 (2013).
22. J. S. Speagle, C. L. Steinhardt, P. L. Capak, J. D. Silverman, *The Astrophysical Journal Supplement Series* **214**, 15 (2014).
23. N. Haring, H. Rix, *The Astrophysical Journal* **604**, L89 (2004).
24. R. C. E. van den Bosch, *et al.*, *Nature* **491**, 729 (2012).

25. E. Emsellem, *Monthly Notices of the Royal Astronomical Society* **433**, 1862 (2013).
26. I. K. Baldry, *et al.*, *Monthly Notices of the Royal Astronomical Society* **421**, 621 (2012).
27. J. L. Walsh, A. J. Barth, L. C. Ho, M. Sarzi, *Astrophysical Journal* **770**, 86 (2013).
28. K. Gebhardt, *et al.*, *The Astrophysical Journal* **729**, 119 (2011).
29. C. Y. Peng, *et al.*, *The Astrophysical Journal* **649**, 616 (2006).
30. R. J. McLure, M. J. Jarvis, T. A. Targett, J. S. Dunlop, P. N. Best, *Monthly Notices of the Royal Astronomical Society* **368**, 1395 (2006).
31. I. S. McLean, *et al.*, *SPIE Conference Series* **8446**, J84460–1-15 (2012).
32. W. D. Vacca, M. C. Cushing, J. T. Rayner, *Publications of the Astronomical Society of the Pacific* **115**, 389 (2003).
33. M. C. Cushing, W. D. Vacca, J. T. Rayner, *Publications of the Astronomical Society of the Pacific* **116**, 362 (2004).
34. H. J. McCracken, *et al.*, *Astronomy and Astrophysics* **544**, A156 (2012).
35. H. Netzer, B. Trakhtenbrot, *The Astrophysical Journal* **654**, 754 (2007).
36. Y. Shen, *et al.*, *The Astrophysical Journal Supplement Series* **194**, 45 (2011).
37. B. Trakhtenbrot, H. Netzer, *Monthly Notices of the Royal Astronomical Society* **427**, 3081 (2012).
38. T. A. Boroson, R. F. Green, *The Astrophysical Journal Supplement Series* **80**, 109 (1992).
39. K. D. Denney, *et al.*, *The Astrophysical Journal* **775**, 60 (2013).

40. J. W. Sulentic, P. Marziani, D. Dultzin-Hacyan, *Annual Review of Astronomy and Astrophysics* **38**, 521 (2000).
41. B. M. Peterson, *et al.*, *The Astrophysical Journal* **613**, 682 (2004).
42. R. Zamanov, *et al.*, *The Astrophysical Journal* **576**, L9 (2002).
43. T. A. Boroson, *The Astronomical Journal* **130**, 381 (2005).
44. S. Komossa, D. Xu, H. Zhou, T. Storchi-Bergmann, L. Binette, *The Astrophysical Journal* **680**, 926 (2008).
45. M. Elvis, *et al.*, *The Astrophysical Journal* **759**, 6 (2012).
46. E. Lusso, *et al.*, *Astronomy and Astrophysics* **534**, A110 (2011).
47. G. T. Richards, *et al.*, *The Astrophysical Journal Supplement Series* **166**, 470 (2006).
48. G. Bruzual, S. Charlot, *Monthly Notices of the Royal Astronomical Society* **344**, 1000 (2003).
49. G. Chabrier, *Publications of the Astronomical Society of the Pacific* **115**, 763 (2003).
50. L. Silva, R. Maiolino, G. L. Granato, *Monthly Notices of the Royal Astronomical Society* **355**, 973 (2004).
51. D. Lutz, *et al.*, *Astronomy and Astrophysics* **532**, A90 (2011).
52. I. Aretxaga, *et al.*, *Monthly Notices of the Royal Astronomical Society* **415**, 3831 (2011).
53. D. A. Dale, G. Helou, *The Astrophysical Journal* **576**, 159 (2002).
54. H. Netzer, *et al.*, *The Astrophysical Journal* **666**, 806 (2007).

55. M. C. Bentz, *et al.*, *The Astrophysical Journal* **767**, 149 (2013).
56. S. Kaspi, *et al.*, *The Astrophysical Journal* **629**, 61 (2005).
57. M. C. Bentz, B. M. Peterson, H. Netzer, R. W. Pogge, M. Vestergaard, *The Astrophysical Journal* **697**, 160 (2009).
58. C. J. Grier, *et al.*, *The Astrophysical Journal* **773**, 90 (2013).
59. J.-H. Woo, *et al.*, *The Astrophysical Journal* **772**, 49 (2013).
60. P. Marziani, J. W. Sulentic, I. Plauchu-Frayn, A. del Olmo, *Astronomy and Astrophysics* **555**, A89 (2013).
61. P. Marziani, J. W. Sulentic, G. M. Stirpe, S. Zamfir, M. Calvani, *Astronomy and Astrophysics* **495**, 83 (2009).
62. A. Marconi, *et al.*, *Monthly Notices of the Royal Astronomical Society* **351**, 169 (2004).
63. D. E. Vanden Berk, *et al.*, *The Astronomical Journal* **122**, 549 (2001).
64. H. Netzer, *The Physics and Evolution of Active Galactic Nuclei* (Cambridge University Press, Cambridge, 2013).
65. S. Bonoli, L. Mayer, S. Callegari, *Monthly Notices of the Royal Astronomical Society* **437**, 1576 (2013).
66. P. Natarajan, *Bulletin of the Astronomical Society of India* **39**, 145 (2011).
67. M. Volonteri, *Science* **337**, 544 (2012).
68. L. Mayer, *et al.*, <http://arxiv.org/abs/1411.5683>.
69. P. Madau, F. Haardt, M. Dotti, *The Astrophysical Journal* **784**, L38 (2014).

70. S. J. Lilly, *et al.*, *The Astrophysical Journal Supplement Series* **172**, 70 (2007).
71. R. J. Weymann, R. F. Carswell, M. G. Smith, *Annual Review of Astronomy and Astrophysics* **19**, 41 (1981).
72. D. M. Crenshaw, S. B. Kraemer, I. M. George, *Annual Review of Astronomy and Astrophysics* **41**, 117 (2003).
73. R. R. Gibson, *et al.*, *The Astrophysical Journal* **692**, 758 (2009).
74. R. Ganguly, *et al.*, *The Astrophysical Journal* **665**, 990 (2007).
75. F. Hamann, *The Astrophysical Journal* **500**, 798 (1998).
76. T. Misawa, *et al.*, *The Astrophysical Journal Supplement Series* **171**, 1 (2007).
77. D. M. Capellupo, F. Hamann, T. A. Barlow, *Monthly Notices of the Royal Astronomical Society* **444**, 1893 (2014).
78. D. Thomas, C. Maraston, R. Bender, C. M. de Oliveira, *The Astrophysical Journal* **621**, 673 (2005).
79. Y.-J. Peng, *et al.*, *The Astrophysical Journal* **721**, 193 (2010).
80. C. L. Carilli, F. Walter, *Annual Review of Astronomy and Astrophysics* **51**, 105 (2013).
81. M. T. Sargent, *et al.*, *The Astrophysical Journal* **793**, 19 (2014).

Acknowledgments

The new MOSFIRE data presented herein were obtained at the W.M. Keck Observatory, which is operated as a scientific partnership among the California Institute of Technology, the University of California and the National Aeronautics and Space Administration. The Observatory

was made possible by the generous financial support of the W.M. Keck Foundation. We thank M. Kassis and the rest of the staff at the W.M. Keck observatories at Waimea, HI, for their support during the observing run. We recognize and acknowledge the very significant cultural role and reverence that the summit of Mauna Kea has always had within the indigenous Hawaiian community. We are most fortunate to have the opportunity to conduct observations from this mountain. Some of the analysis presented here is based on data products from observations made with European Southern Observatory (ESO) Telescopes at the La Silla Paranal Observatory under ESO program ID 179.A-2005 and on data products produced by TERAPIX and the Cambridge Astronomy Survey Unit on behalf of the UltraVISTA consortium. We are grateful to A. Faisst and M. Onodera for their assistance with the acquisition and reduction of the MOS-FIRE data. We thank S. Tacchella, J. Woo, and W. Hartley for their assistance with some of the evolutionary calculations. K.S. gratefully acknowledges support from Swiss National Science Foundation Professorship grant PP00P2_138979/1. F.C. acknowledges financial support by the NASA grant GO3-14150C. M.E. acknowledges financial support by the NASA *Chandra* grant GO2-13127X. B.T. is a Zwicky Fellow at the ETH Zurich.

The Supplementary Materials, available on Science Online, include:

Data, Methods, and Supplementary Text S1 to S5

Figs. S1 to S4

Table S1

References (31-81)

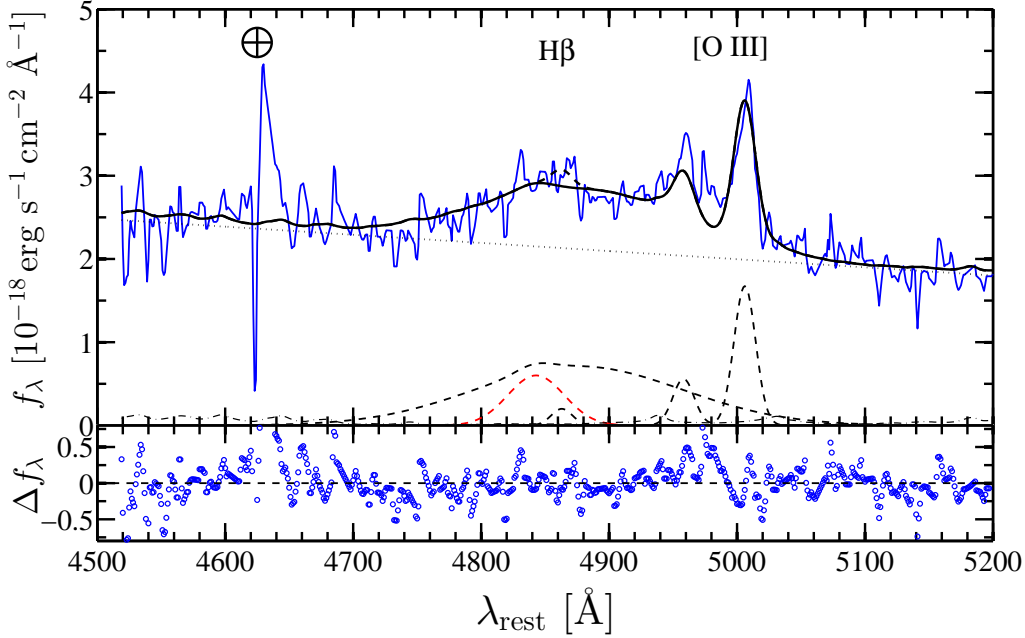


Figure 1: **The observed Keck/MOSFIRE spectrum and best-fit model for the $H\beta$ emission complex of CID-947.** The data are modeled with a linear continuum (dotted), a broadened iron template (dot-dashed) and a combination of broad and narrow Gaussians (dashed), which correspond to the $H\beta$ and $[O\ III]$ emission lines (see section S1.2 in the supplementary materials for details regarding the spectral modeling). The broad component of $H\beta$ has a full width at half maximum of $\text{FWHM}(H\beta) = 11330\text{ km s}^{-1}$, which results in $M_{\text{BH}} = 6.9 \times 10^9 M_{\odot}$ and $M_{\text{BH}}/M_* = 1/8$. The red dashed line illustrates an alternative scenario, in which the SMBH mass derived from the $H\beta$ line width would result in $M_{\text{BH}}/M_* = 1/100$ [i.e., $\text{FWHM}(H\beta) = 3218\text{ km s}^{-1}$], clearly at odds with the data. The spike at $\lambda_{\text{rest}} \simeq 4640\text{ \AA}$ is due to a sky feature. The bottom panel shows the residuals of the best fit model.

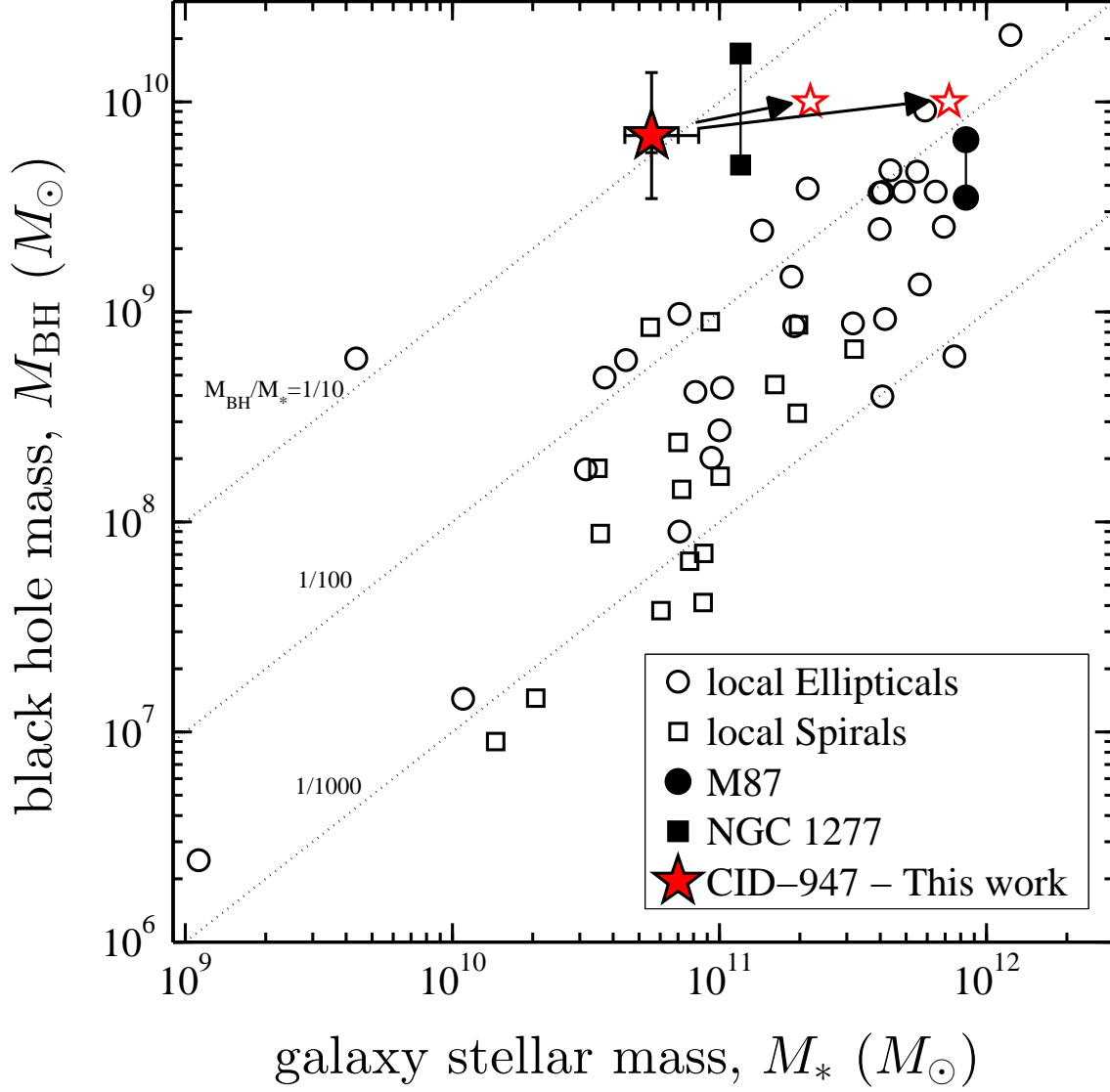


Figure 2: **A comparison of CID-947 with a compilation of observed M_{BH} and M_* estimates in the local universe** [adapted from (4), assuming the tabulated bulge-to-total fractions]. CID-947 (red star) has a very high BH-to-stellar mass ratio of $M_{\text{BH}}/M_* \simeq 1/10$. The asymmetric error bars shown on M_{BH} and M_* represent measurement-related uncertainties, while the symmetric ones demonstrate systematic uncertainties of 0.3 dex (on M_{BH}) and 0.1 dex (on M_*). The masses inferred for subsequent growth scenarios are highlighted as empty red stars. The CID-947 system is expected to evolve only mildly in M_{BH} (perhaps to $\sim 10^{10} M_\odot$), but M_* should grow to at least $2 \times 10^{11} M_\odot$, and possibly to as much as $\sim 7 \times 10^{11} M_\odot$, by $z = 0$. The local galaxies NGC 1277 and M87, which could be considered as descendants of systems like CID-947, are highlighted as filled symbols [(25) and (27), respectively]. Some studies suggest these galaxies to have somewhat higher M_{BH} , and therefore relatively high mass ratios, of $M_{\text{BH}}/M_* = 1/7$ and $1/127$, respectively (24, 28).

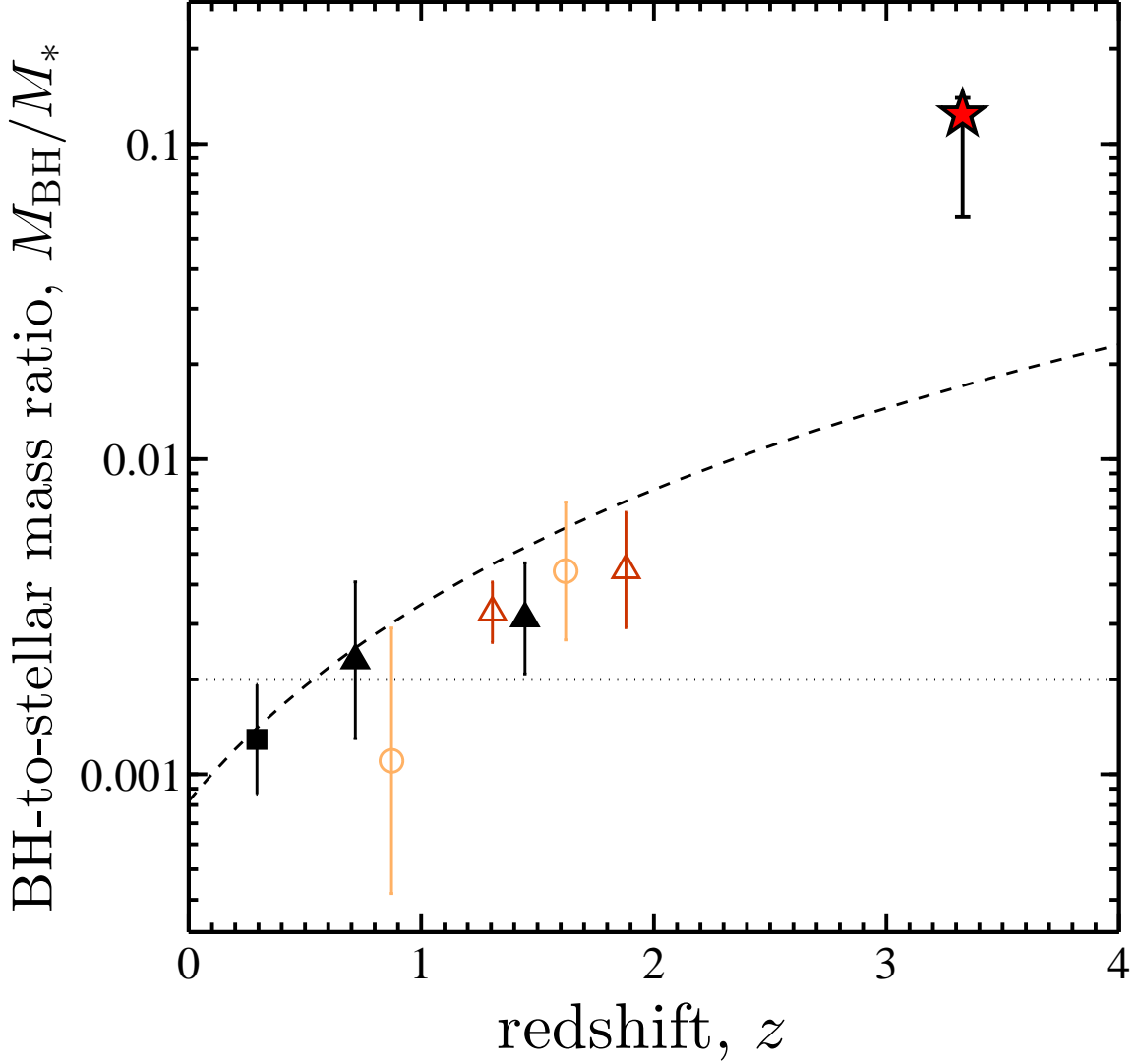


Figure 3: **The observed cosmic evolution of the BH-to-stellar mass ratio, M_{BH}/M_* , and its extrapolation beyond $z \sim 2$.** CID-947 (red star) has $M_{\text{BH}}/M_* = 1/8$ at $z \simeq 3.3$, which is higher by a factor of at least ~ 50 than the typical value in local, inactive galaxies (at most, $M_{\text{BH}}/M_* \sim 1/500$; dotted line). The error bars shown for CID-947 represent only the measurement-related uncertainties, propagating the uncertainties on M_{BH} and on M_* . The different data points at $z < 2$ represent typical (median) values for several samples with M_{BH}/M_* estimates, with uncertainties representing the scatter within each sample [filled symbols, open circles, and open triangles represent samples from (7), (29), and (6), respectively; adapted from (7)]. Even compared to the extrapolation of the evolutionary trend supported by these lower-redshift data, $M_{\text{BH}}/M_* \sim (z + 1)^2$ [dashed line, scaled as in (30)], CID-947 has a significantly higher M_{BH}/M_* .

Supplementary Materials for
An Over-Massive Black Hole in a Typical Star-Forming Galaxy, 2 Billion
Years After the Big Bang

Authors: Benny Trakhtenbrot,*
C. Megan Urry, Francesca Civano, David J. Rosario, Martin Elvis, Kevin Schawinski, Hyewon
Suh, Angela Bongiorno, Brooke D. Simmons

*To whom correspondence should be addressed; E-mail: benny.trakhtenbrot@phys.ethz.ch

This PDF file includes:

Data, Methods and Supplementary Text §§S1-S5
Figures S1 to S4
Table S1
Additional references 31 to 81

In these Supplementary Materials, we provide additional details about all the aspects of our study presented and discussed in the main article, including: the new Keck/MOSFIRE K -band observations and their analysis (§S1); the multiwavelength data and related derivation of stellar mass (M_*) and star formation rate (SFR; §S2); the derivation of black hole mass (M_{BH}) and accretion rate (L/L_{Edd}), and a discussion of the SMBH evolution (§S3); the rest-frame UV spectrum, broad absorption features and properties of the AGN-driven outflow (§S4); and of the calculations of possible final M_* of the host galaxy (§S5).

S1 New Keck/MOSFIRE K -band Data and Analysis

S1.1 Keck/MOSFIRE Observations and Data Reduction

The source CID–947 (J2000.0 coordinates $\alpha = 10:01:11.35$, $\delta = +02:08:55.6$) was observed with the Keck/MOSFIRE instrument (31) during the night of January 23–24th., 2014, with observing time allocated through the Yale-Caltech collaborative agreement. We used the normal K -band setup, which covers order 4 of the 110.5 mm^{-1} reflection grating. As CID–947 was our primary target, it was positioned near the center of the mask, providing a spectral coverage of $\lambda = 19,415\text{--}23,837 \text{ \AA}$. To ensure adequate coverage of the sky background emission, and its subtraction from the AGN signal, we used 4 pairs of MOSFIRE bars, to form a $24''$ -long pseudo-slit. The MOSFIRE pixel scale is $0.18''/\text{pix}$. To prevent significant slit losses, we set the slit width(s) to $1''$, which resulted in a spectral resolution of about $R \equiv \lambda/\Delta\lambda = 3600$. Observational conditions during the night were generally good, with typical seeing of $\sim 0.8''$ in the K -band during the science observations. The science exposures, totaling an hour, consisted of 20 separate sub-exposures of 3 minutes each, dithered between two positions along the slit with a separation of $4''$, to allow for an accurate subtraction of the sky emission. The typical airmass during the observations was about 1.08. Several times during the night we also observed the A0v stars HIP-34111 and HIP-56736, as well as the fainter white dwarf GD71, to allow a

robust flux calibration.

The data were reduced using a combination of different tools. First, we used the dedicated MOSFIRE pipeline (2014.06.10 version) to obtain flat-fielded, wavelength calibrated 2D spectra of all the sources observed within each mask (including the standard stars). The wavelength calibration was performed using sky emission lines, and the best-fit solutions achieved an rms of $\sim 0.1\text{\AA}$. Next, we used standard IRAF procedures to produce a 1D spectrum, using an aperture of 11 pix (i.e., $2''$). Finally, we used the `Spextool` IDL package to remove the telluric absorption features near $2\text{ }\mu\text{m}$ and to perform the relative and absolute flux calibrations, based on a detailed library spectrum of Vega (32, 33). The absolute flux calibration we obtained is in excellent agreement with the archival photometry available for CID-947: the synthetic magnitude derived from the spectrum is $K_s = 20.03$ (AB magnitudes), compared with the archival value of 20.00 ± 0.01 (34). We however chose to apply the minor scaling needed to match the archival photometry (a factor of 1.03), in order to be fully consistent with the value used in the SED decomposition (§S2). We finally note that CID-947 is one of several COSMOS targets observed in this campaign, and we verified the robustness of the different reduction steps by visually verifying that the same reduction yields artifact-free spectra for the other sources. The typical signal-to-noise across the core part of the spectrum is $S/N \sim 5 - 7$ per pixel. After re-binning the spectrum to a uniform spacing of $1\text{ }\text{\AA}$ (in rest-frame; 60 km s^{-1}), we obtain $S/N \sim 7 - 10$ per spectral resolution element.

S1.2 Spectral Analysis of $\text{H}\beta$ Emission Complex

We modeled the K -band spectrum of CID-947 to measure the monochromatic continuum luminosity at (rest-frame) wavelength of 5100\AA ($\lambda L_\lambda [5100\text{\AA}]$, or L_{5100}) and the width of the broad $\text{H}\beta$ emission line (FWHM ($\text{H}\beta$)). The analysis methodology is very similar to that discussed in numerous previous works (e.g., (35–37), and references therein), and is only briefly described

here.

The spectra were modeled with a linear (pseudo) continuum, a broadened Fe II template (38), and a combination of Gaussians which account for the broad and narrow emission lines, namely $H\beta$, [O III] $\lambda\lambda 4959, 5007$, and He II $\lambda 4686$. The $H\beta$ model consists of a broad component (modeled with 2 Gaussians) and a narrow component, which is tied to the width of the [O III] lines. The continuum flux at 5100\AA was estimated directly from the best-fit linear continuum.¹ We preferred to use FWHM over σ_{BLR} as the probe of the virial velocity field of the BLR gas, as the former can be more robustly estimated in spectra of limited S/N, as is the case with our MOSFIRE data (39). However, since the best-fitting model for $H\beta$ turned out to be overwhelmingly dominated by a single broad Gaussian component (the flux ratio between the two components is 45:1), the differences between the results derived by two approaches are expected to be negligible. The best-fit models are presented in Figure S1. The relevant best-fit parameters resulting from our fitting of the MOSFIRE spectrum are $\text{FWHM}(H\beta) = 11330 \text{ km s}^{-1}$, and $L_{5100} = 4.16 \times 10^{45} \text{ erg s}^{-1}$. After accounting for host-galaxy contamination of about 14% (following the analysis presented in §S2), the intrinsic optical luminosity becomes $L_{5100} = 3.58 \times 10^{45} \text{ erg s}^{-1}$. We note that the broad $H\beta$ profile in our best-fit model is highly symmetric, with an asymmetry index of $\text{A.I.} = 0.03$, consistent with the typical value found in large samples of un-obscured AGN (see, e.g., (40)). The broad component is, however, blue-shifted by about 830 km s^{-1} , relative to the expected wavelength (at the source systemic redshift). Such large blue-shifts are relatively rare, with an occurrence rate of only about 5%.² To verify that our estimate of $\text{FWHM}(H\beta)$ is not severely affected by these properties of broad $H\beta$ profile, we obtained an alternative estimate of the line width, which relies only on the blue part of the profile, which is not blended with Iron and [O III] emission.

¹The monochromatic luminosity, as all other luminosities and ages reported here, are calculated assuming a cosmological model with $\Omega_{\Lambda} = 0.7$, $\Omega_{\text{M}} = 0.3$, and $H_0 = 70 \text{ km s}^{-1} \text{ Mpc}^{-1}$.

²This estimate is based on the $H\beta$ measurements of about 20,000 SDSS AGN, presented in Ref. (37).

This alternative estimate is obtained by doubling the one-sided line width, which was measured following the approach described in Ref. (41). This results in a FWHM ($H\beta$)-equivalent of 9236 km s^{-1} , only 0.09 dex lower than our best-fit value. However, we stress that this alternative estimate is far less robust than our fiducial, best-fit value, as it relies on the identification of the (spectral) pixel with maximal flux density, which is very sensitive to small-scale flux density fluctuations in spectra of limited S/N, as in the present case. We conclude that our estimate of the width of the broad component of $H\beta$ is not significantly affected by the shape or shift.

Due to the complexity of the spectral fitting procedure, the best approach to derive the measurement-related uncertainties on L_{5100} and FWHM ($H\beta$) (and therefore on M_{BH} ; see §S3 below) is via re-sampling of the data. To this end, we constructed a set of 500 artificial spectra, by adding normally-distributed random noise to the observed spectra of CID-947, scaled to provide either $S/N = 10$ (comparable to the noise level in the observed data). An additional set of 500 simulations assumed a more conservative noise level of $S/N = 5$, to verify that our results are not driven by an under-estimation of the noise level in the data. We then re-fitted each of these artificial spectra, using the same fitting procedure as described above. The resulting best-fitting models are illustrated in the top panel of Figure S1. After measuring L_{5100} and FWHM ($H\beta$) for each of these best-fitting models, we obtained an artificial sample of FWHM ($H\beta$) values, the cumulative distribution function of which is illustrated in the lower-left panel of Fig. S1. Fig. S1 clearly demonstrates that, even under the conservative assumption of $S/N = 5$, about 95% of our simulations resulted in $\text{FWHM}(H\beta) \gtrsim 8600 \text{ km s}^{-1}$. This conservative lower limit on FWHM ($H\beta$) is lower than the best-fit value by about 0.14 dex.

The spectral region adjacent to the [O III] lines may suggest that their profiles may include an additional broad component (i.e., a “blue wing”). We therefore performed yet another set of simulations, with an alternative version of the fitting procedure that allows for an additional broad component for [O III]. The broad components for the two [O III] lines were forced

to share a common width (in the range $500 - 1400 \text{ km s}^{-1}$) and relative shift (in the range $-350 - +150, \text{ km s}^{-1}$). These limits are motivated by the distributions of line widths and shifts found for large samples of un-obscured AGN (e.g., (42–44)). The results of the simulations indicate that this adjustment to the [O III] profiles does not systematically affect our estimate of FWHM ($\text{H}\beta$). The median value obtained in the simulations is $\text{FWHM}(\text{H}\beta) = 10150 \text{ km s}^{-1}$, and 95% of the simulations resulted in $\text{FWHM}(\text{H}\beta) > 6740 \text{ km s}^{-1}$.

S2 Broad-band Spectral Energy Distribution and Estimates of L_{bol} , M_* and SFR

We used the available multiwavelength data for CID–947 to determine the bolometric luminosity (L_{bol}) of the AGN in CID–947, and the stellar mass (M_*) and star formation rate (SFR) of the host galaxy. The broad-band spectral energy distribution (SED) for CID–947 includes data from a large variety of surveys of the COSMOS field, including data in the X-ray (*Chandra* and *XMM-Newton*), optical-to-near-IR (Subaru and CFHT), mid-to-far-IR (*Spitzer* and *Herschel*), and millimeter (JMCT) regimes.

The broad-band SED of CID–947 was analyzed in previous studies of COSMOS AGN, which derived and reported estimates of L_{bol} . One such analysis, based on *Chandra* X-ray data (45), yields $L_{\text{bol, SED}} = 1.31 \times 10^{46} \text{ erg s}^{-1}$ (correcting for our adopted cosmology).³ Another study, based on *XMM-Newton* X-ray data (ref. (46); XMM-ID 60131), gives $L_{\text{bol, SED}} = 1.81 \times 10^{46} \text{ erg s}^{-1}$ (also cosmology-corrected). The difference between these two values, of a factor of 1.6, is mostly due to the markedly different X-ray fluxes reported for CID–947 in the *Chandra* and *XMM-Newton* surveys of the COSMOS field, which may be due to intrinsic source variability. We note that the stellar component in the SED (see below) has a negligible

³Here we use the luminosity integrated between 40 keV and $1 \mu\text{m}$, to avoid double-counting the re-processed mid-IR emission (which would add about 17% to L_{bol} for CID–947).

contribution to these estimates of L_{bol} (i.e., $< 1\%$).

To derive the host galaxy properties, the SED of CID-947 was modeled separately for the rest-frame UV-optical-NIR, and for the Mid-IR-to-millimeter regime.

The rest-frame UV-optical-NIR part of the SED includes the emission from the accreting SMBH, a part of which is re-processed by a dusty toroidal structure (“torus”) and re-emitted in IR wavelengths, and from stellar population of the host galaxy. The data in this regime consists of flux measurements in 13 spectral bands (obtained with Subaru, CFHT and *Spitzer*), ranging from $\sim 3700 \text{ \AA}$ (CFHT/ u^*) to $24 \text{ }\mu\text{m}$ (*Spitzer*/MIPS). We first rely on the data accumulated and analyzed in a previous COSMOS study by Bongiorno et al. (20). Here we mention briefly only some of the features of this modeling, and refer the reader to (20) for a detailed discussion. In that study, the data were modeled as the sum of two distinct components, representing the emission originating from the AGN and from stars in the host galaxy. The AGN component is described by the multiwavelength AGN SED of Richards et al. (2006; (47)). The stellar component was described by a grid of models, produced by a well-established stellar popular synthesis procedure (48). Each of the templates represents a stellar population with a different age (ranging from 50 Myr - 1.88 Gyr) and exponential decay rate ($\tau_{\text{SFH}} = 0.1 - 30 \text{ Gyr}$), and further assume a Chabrier initial mass function (49). The templates were then subjected to both nuclear and galaxy-wide dust extinction (with $E_{\text{B-V}}$ values of up to 1 and 0.5, respectively). The best-fit model for CID-947 in the Bongiorno et al. study (Fig. S2, left) provides a stellar mass of $M_* = 5.57^{+2.78}_{-0.38} \times 10^{10} M_{\odot}$, with a reddening of $E_{\text{B-V}} = 0.5$. The fraction of the total monochromatic luminosity at 5100 \AA which is contributed by the stellar component is about $f_{\text{host}}(5100) = 0.14$. This host contamination is taken into account when we estimate the mass of the SMBH (see §S3).

We have repeated the UV-to-IR SED fitting, using the most up-to-date imaging data available for CID-947 (UltraVISTA DR2, (34); see Table S1), and a slightly modified AGN model,

in which the emission from the dusty torus (dominating the mid-IR regime) is separated from the intrinsic AGN radiation (dominating the UV-optical regime). Our analysis resulted in a very similar stellar mass to the aforementioned one. The stellar component is represented, as before, by the Richards et al. AGN SED, which is however extrapolated as a power-law at $\lambda_{\text{rest}} > 4000$ Å. The IR emission from the dusty torus is represented by composites from a dedicated study of the IR SEDs of AGN (50). The grid of stellar population models have remained the same as in the aforementioned “reference” SED fit, with the age of the stellar population capped at the age of the Universe at $z = 3.328$. Our choice of the Bruzual & Charlot models is motivated by the fact that they were also used in most studies of star forming galaxies at $z > 3$, which we use here as reference (e.g., (21, 22)). For a detailed discussion of the effects of alternative stellar population models, e.g., (21) and (22). We have restricted the components so that the UV-optical part of the SED would be dominated by the AGN, i.e. $f_{\text{AGN}} > f_{\text{host}}$. This is motivated by the overall AGN luminosity of CID-947 (see above) and the fact that the rest-frame UV spectrum does not show significant host contamination in the deep absorption features (see §S4). We have also explicitly omitted the data below $\lambda_{\text{rest}} = 1216$ Å (i.e., the u and B bands), as these are expected to be affected by Ly α absorption by the intergalactic medium along the line of sight to CID-947. The resulting additional best-fit model (Fig. S2, right) relies on a stellar population with an age of 1 Gyr, a stellar mass of $M_* = 4.37^{+0.42}_{-0.48} \times 10^{10} M_{\odot}$, with a reddening of $E_{B-V} = 0.05$. In this new fit, the stellar component contributes $f_{\text{host}}(5100) = 0.36$. Next, we re-fitted the data with a restricted model in which the stellar population is kept at the oldest reasonable age (1.8 Gyr). Since older stellar populations have higher mass-to-light ratios, such a fit would in principle provide a conservative upper limit on the stellar mass. This fit resulted in $M_* = 6.48^{+0.28}_{-0.56} \times 10^{10} M_{\odot}$, and $f_{\text{host}}(5100) = 0.35$. Finally, we have repeated this oldest-population fit, this time without the restriction of $f_{\text{AGN}} > f_{\text{host}}$. This resulted in $M_* = 5.95 \pm 0.21 \times 10^{10} M_{\odot}$, and $f_{\text{host}}(5100) = 0.55$. We stress however that these latter

age-restricted models do *not* provide the best fits of the data, as the resulting χ^2 is higher than that found for the non-restricted case. We conclude that the best-fit stellar mass that we obtain for the host of CID-947 is $M_* = 4.37 \pm_{-0.48}^{+0.42} \times 10^{10} M_\odot$. We however choose to base the rest of the analysis on the slightly higher mass found in the Bongiorno et al. study, as it represents a more conservative choice given the extremely high BH-to-stellar mass ratio we find for CID-947, and since it is based on the same SED decomposition code that was used in some of the reference studies to which we compare our results (6).

The Mid-IR-to-millimeter part of the SED is dominated by emission from the (cold) dusty gas in the host galaxy, heated by the star formation activity. Here we rely on *Herschel* and JMCT/AzTEC detections at 500 μm and 1.1 millimeter, and upper limits at 100, 160, 250 and 350 μm , from *Herschel* (51, 52). The data were fit with a grid of dust-emission templates of star-forming galaxies, covering a representative range of SED shapes (i.e., effective temperatures; (53)). The best-fit template for the far-IR and millimeter data implies a star formation rate of $\text{SFR} = 392 M_\odot \text{yr}^{-1}$. We present the Mid-IR-to-millimeter data and models in Fig. S3. We stress that the AGN contribution to the emission in this regime is negligible, as demonstrated by the dotted black line in Fig. S3 (54). The SFR estimate relies on low-resolution *Herschel* and JMCT/AzTEC measurements, and therefore may be contaminated (confused) by emission originating from neighboring (unrelated) sources.

S3 Determination of black hole mass and accretion rate, and the past evolution of the SMBH

Using the best-fit values for L_{5100} and FWHM ($\text{H}\beta$) (see §S1.2 above), and applying commonly-used virial estimators of M_{BH} (10, 37), we obtain $M_{\text{BH}} = 6.91 \times 10^9 M_\odot$. Alternative calibrations of such virial mass estimators do not alter our findings significantly. For example, the calibration obtained by a recent reverberation mapping study (55) implies $M_{\text{BH}} = 5.68 \times 10^9 M_\odot$;

that is, smaller than our fiducial measurement by less than 0.1 dex. We use the simulations described above (§S1.2) to estimate the measurement uncertainties on M_{BH} . The best-fitting L_{5100} and FWHM ($\text{H}\beta$) for each simulated spectrum were combined to provide a set of artificial estimates of M_{BH} . The cumulative distribution function of these M_{BH} estimates is presented in the lower-right panel of Fig. S1. For the $S/N = 10$ simulations we find that the 16% and 84% quantiles are at 5.73×10^9 and $7.66 \times 10^9 M_{\odot}$, respectively, resulting in 1σ -equivalent uncertainties on M_{BH} of -1.18×10^9 and $+0.75 \times 10^9 M_{\odot}$. We further find that 95% (99%) of these simulations resulted in $M_{\text{BH}} > 5.09 \times 10^9 M_{\odot}$ ($3.61 \times 10^9 M_{\odot}$). The corresponding values for the $S/N = 5$ simulations are $M_{\text{BH}} > 3.82 \times 10^9$ and $2.96 \times 10^9 M_{\odot}$, respectively. Virial (or “single-epoch”), $\text{H}\beta$ -based estimates of M_{BH} are also known to be prone to systematic uncertainties, of up to ~ 0.4 dex, due to the reliance on the empirical $R_{\text{BLR}} - L_{5100}$ relation, and the overall normalization of the mass estimators. We stress however that our analysis of CID–947 should, in principle, suffer *less* from systematics, compared to similar studies of more luminous sources at $z \sim 3.5$, as its luminosity of $L_{5100} = 3.4 \times 10^{45} \text{ erg s}^{-1}$ lies within the range covered directly by reverberation mapping experiments (55–57). The leading systematic uncertainty in the present case is therefore associated with the assumption of a typical “geometrical factor” (commonly referred to as f_{BLR}), which is of order 0.1 dex (58, 59).

Another source of concern is the possibility that the BLR is observed at a high inclination angle, as suggested by the presence of the broad *absorption* features (i.e., BAL features) in the rest-frame UV part of the spectrum of CID–947 (see §S4 below). One may suspect that in such a case, the measured FWHM ($\text{H}\beta$) would systematically over-estimate the typical velocity dispersion in the BLR, and thus lead to an overestimated M_{BH} . We have investigated this issue by comparing the distributions of FWHM (Mg II) in large samples of non-BAL QSOs, and those with a BAL feature in the $\text{C IV } \lambda 1549$ line (as in CID–947), among sources at $1.6 < z < 1.9$, drawn from a large catalog based on the Sloan Digital Sky Survey (36). Although in the

current work we used $H\beta$, and not the $\text{Mg II } \lambda 2798$ line as our virial estimator, the widths of these two lines have been shown to be closely correlated, and they are thought to originate from a similar region within the BLR (e.g., (36, 37)). The distributions of FWHM (Mg II) for BAL and non-BAL QSOs (1723 and 15370 objects, respectively) are very similar in shape, with the median FWHM value for BAL QSOs being only slightly higher, by merely 230 km s^{-1} . Moreover, there is no excess of BAL QSOs with line widths comparable to what we estimate for CID-947 (i.e., $\gtrsim 10,000 \text{ km s}^{-1}$).

Several phenomenological studies have raised the possibility that, for *some* luminous sources with particularly broad $H\beta$ lines ($\text{FWHM}(H\beta) \gtrsim 4000 \text{ km s}^{-1}$), the line profiles might include a significant contribution from a non-virialized “very broad component”, which should not be taken into account when estimating M_{BH} (e.g., (60)). Simply adopting the empirically derived (and perhaps luminosity-dependent) corrections suggested in such studies (60, 61), our estimate for M_{BH} should be scaled down by about 0.2-0.25 dex. In the context of our main finding, of an extremely high BH-to-stellar mass ratio for CID-947, this would mean $M_{\text{BH}}/M_* \simeq 1/15 - 1/12$ - still a very high value (see Fig. 3). We however stress that the commonly advocated approach to singling out such peculiar objects is based on the unambiguous identification of two components in the broad $H\beta$ emission line (the “core” and the “very broad component”), as well as some line asymmetry. Since the $H\beta$ profile in CID-947 does not show such a complicated structure, the aforementioned empirical corrections should not be applied.

Finally, the alternative, “one sided” estimate of the line width (see §S1.2 above) would translate to a decrease of about 0.18 dex in any “virial” estimate of M_{BH} . As explained in §S1.2, and demonstrated in our simulations, this is not a robust estimate of the line width. We note, however, that such a decrease in M_{BH} would have a similar effect on our main result as the one discussed above, namely providing $M_{\text{BH}}/M_* \simeq 1/12$.

We conclude that the SMBH powering the AGN in CID-947 has a mass of $M_{\text{BH}} > 3.6 \times$

$10^9 M_\odot$, at the 99% confidence level, and our best estimate is $M_{\text{BH}} = 6.9 \times 10^9 M_\odot$.

The rest-frame optical spectrum was used to derive yet another estimate of L_{bol} , by applying a bolometric correction (i.e., $f_{\text{bol}}(5100\text{\AA}) \equiv L_{\text{bol}}/L_{5100}$). This approach is consistent with many previous studies of un-obscured AGN, at all redshifts. We used the luminosity-dependent prescription described in (37), which in turn relies on the B -band bolometric corrections presented in (62), translated to 5100 Å assuming a UV-optical SED with $f_\nu \propto \nu^{-1/2}$ (63). For CID-947, this results in $L_{\text{bol, opt}} = 2.11 \times 10^{46} \text{ erg s}^{-1}$. This value is highly consistent with the *XMM-Newton*-based estimate of $L_{\text{bol, SED}}$ (ref. (46); within 0.06 dex), but significantly higher than the *Chandra*-based value (ref. (45); by a factor of almost 2).

The derived values of L_{bol} and M_{BH} were combined to provide estimates of the normalized accretion rate, in terms of the Eddington luminosity, $L/L_{\text{Edd}} \equiv L_{\text{bol}}/(1.5 \times 10^{38} M_{\text{BH}}/M_\odot)$ (this definition of the “Eddington ratio” assumes a Solar gas-phase metallicity). We obtain $L/L_{\text{Edd}} = 0.021$ for the L_{5100} -based estimate of L_{bol} , or 0.019 and 0.011 for the *XMM-Newton* and *Chandra*-based estimates of $L_{\text{bol, SED}}$, respectively. Given the fact that the estimates of L_{bol} were obtained using very different approaches, and the systematic uncertainties associated with the estimation of L_{bol} (e.g., the scatter in $f_{\text{bol}}(5100\text{\AA})$), we consider these estimates of L/L_{Edd} to be in excellent qualitative agreement: the SMBH in CID-947 is accreting at a rate of at most $L/L_{\text{Edd}} \simeq 0.02$.

By combining the estimated L/L_{Edd} and a standard radiative efficiency of $\eta = 0.1$ (62), we obtain an e -folding timescale for the growth of the SMBH, following the expression $\tau_{\text{BH}} = 4 \times 10^8 \frac{\eta/(1-\eta)}{L/L_{\text{Edd}}} \text{ yr}$. The resulting timescales are about 2.1 and 4 Gyr, for the higher (L_{5100} -based) and lower (*Chandra*-based) estimates of L/L_{Edd} , respectively. In any case, these timescales are longer than the age of the Universe at $z = 3.328$, of about 1.88 Gyr, and than the elapsed time since the earliest seed black holes likely formed, 1.7 Gyr ($z \sim 20$). This very long timescale thus suggests that the SMBH in CID-947 had to experience an earlier epoch of much faster

growth (i.e., higher accretion rate), and/or that it had to originate from the most massive type of seeds. In particular, extrapolating the growth history “backwards” to $z = 10$, assuming constant accretion rate and radiative efficiency of $L/L_{\text{Edd}} = 0.02$ and $\eta = 0.1$ (respectively), results in $M_{\text{BH}}(z = 10) \simeq 3.7 \times 10^9 M_{\odot}$. Even with the lowest efficiency within the framework of a geometrically-thin, optically thick accretion disk, $\eta = 0.038$ (maximally retrograde spinning BH; e.g., (64)), the implied mass is still about $10^9 M_{\odot}$. The most extreme BH seed production mechanisms rely on different “direct collapse” scenarios, but generally provide very few seeds as massive as $M_{\text{seed}} \sim 10^6 M_{\odot}$ (see, e.g., (65) and reviews in (19, 66, 67)). Some very recent studies speculate that *some* BH seed masses may be yet higher, perhaps up to $\sim 10^8 M_{\odot}$, but not before $z = 10$ (68). Considering the accretion rate onto the SMBH, some recent models highlight the possibility of yet more efficient accretion, as the disk becomes “slim” and surpasses the simplified (spherical) Eddington limit, perhaps reaching $\dot{M}/M_{\text{Edd}} \sim 3$ (69). We note however that such extreme models for BH seed production and accretion may not necessarily be required to explain objects like CID–947. The implied M_{BH} of CID–947 at $z \sim 5$, of about $3 \times 10^9 M_{\odot}$, is consistent with that observed in the population of high-luminosity quasars at that epoch (11, 12). Such sources, however, have much higher accretion rates, typically $L/L_{\text{Edd}} \gtrsim 0.5$, and can emerge from standard accretion (at relatively high duty cycles and low radiative efficiency), from a broad range of BH seed masses, including those of stellar remnants (i.e., $M_{\text{seed}} \lesssim 10^3 M_{\odot}$). We stress that in any case, CID–947 had to have higher-than-observed accretion rate *sometime* in the past, to account for its high mass. As we show in §S4 below, we have evidence that this epoch of high accretion rate took place relatively shortly before the observed epoch.

S4 Rest-frame UV spectrum and BAL features

An optical spectrum of CID-947 was obtained as part of the zCOSMOS survey (ref. (70); zCOSMOS-ID 823936), and we present it in Fig. S4. It clearly shows very broad and deep absorption troughs blue-ward of the Si IV $\lambda 1400$ and C IV $\lambda 1549$ lines, identifying CID-947 as a Broad Absorption Line Quasar, a sub-population that comprises about 10-20% of luminous, un-obscured AGN (BALQSOs; see, e.g., (71–73), and references therein). Moreover, the absorption feature blue-ward of the Al III $\lambda 1857$ line suggests that CID-947 may belong to the yet rarer sub-class of low-ionization BAL QSOs (i.e., it is a “LoBAL”). For both C IV and Si IV we estimate a maximum outflow velocity of $|v_{\max}| \simeq 12,000 \text{ km s}^{-1}$, with the C IV trough probably slightly broader. While this value of v_{\max} is not uncommon among BALQSOs (73), it is an outlier in the $v_{\max} - L/L_{\text{Edd}}$ plane: virtually all known BALQSOs with comparable v_{\max} have much higher accretion rates, typically $L/L_{\text{Edd}} > 0.1$ (74).

A simple model for the launching of such high-velocity outflows (75, 76) yields a value for the maximum outflow velocity $v_{\max} \simeq 9300 \left(\frac{R_{\text{abs},0.1}}{M_8} \right)^{-1/2} \left(1.5 \frac{f_{0.1}}{N_{22}} L/L_{\text{Edd}} - 0.1 \right)^{1/2} \text{ km s}^{-1}$, where $R_{\text{abs},0.1}$ is the distance of the absorber from the continuum source, scaled to 0.1 pc; M_8 is the SMBH mass, scaled to $10^8 M_{\odot}$; $f_{0.1}$ is the fraction of continuum photons absorbed (or scattered) by the outflowing gas, scaled to 10%; and N_{22} is the absorber column density, scaled to 10^{22} cm^{-2} . Assuming the observed value for M_{BH} , and also $N_{\text{H}} = 10^{22} \text{ cm}^{-2}$, $R_{\text{abs},0.1} = 1$ and $f_{0.1} = 1$, this expression implies that a wind with $v_{\max} \simeq 12,000 \text{ km s}^{-1}$ should have been launched by a SMBH accreting at $L/L_{\text{Edd}} \gtrsim 0.1$, and probably at rates as high as $L/L_{\text{Edd}} \simeq 0.7$ (see (76) for discussion of viable ranges on all parameters). This is significantly higher, by at least an order of magnitude, than the observed value of L/L_{Edd} . We also note that, since within the framework of this model $L/L_{\text{Edd}} \propto R_{\text{abs},0.1}$, the implied accretion rate can easily reach $L/L_{\text{Edd}} \simeq 1$ if the outflow has reached $\sim 1 \text{ pc}$.

The high-velocity outflow was launched at a time $\Delta t \sim R_{\text{abs}}/v_{\text{max}}$ prior to the observed epoch. Even for a conservative assumption of $R_{\text{abs}} \gtrsim 1 \text{ kpc}$ (e.g., ref. (77) and references therein), the implied age of the outflow is about 10^5 years. Any alternative, more realistic assumption regarding R_{abs} would imply an even shorter timescale.

Thus, the relatively high terminal velocity of the observed outflow lends further support to the scenario in which CID-947 was accreting at much higher rates, probably as recently as $\sim 10^5$ years before the observed epoch.

S5 Subsequent evolution of M_*

We estimated the “final” stellar mass of CID-947 ($M_*(z=0)$) in several ways, all of which rely on the observed stellar mass ($5.6 \times 10^{10} M_\odot$) and star formation rate ($\sim 400 M_\odot \text{ yr}^{-1}$). Our calculations assume that we are observing the host galaxy of CID-947 near its peak of star forming activity, and that the SFR can only decline with time.

First, we assume an exponential decline in SFR, with typical e -folding timescales in the range of $\tau = 1 - 2 \text{ Gyr}$. These short timescales are supported by several observational studies which constrain the ages of the stellar populations in massive, low-redshift galaxies (78), and basically implies that the final mass of the galaxy can be approximated by $M_*(z=0) \simeq M_*(z=3.328) + \text{SFR} \times \tau$. These “integrated” masses should be scaled down, by factors of about 1.6, to account for the fact that some of the mass is returned back to the galaxy’s gas (e.g., through stellar winds, Supernovae explosions etc.). Using the observed M_* and SFR for CID-947 we obtain final masses of $M_*(z=0) \simeq (2.8 - 5.3) \times 10^{11} M_\odot$.

An alternative calculation relies on the scenario in which star-forming galaxies evolve on the “main sequence” at all epochs, until they quench, and that the mass functions of such objects, at all epochs, can be linked via the so-called “continuity approach” (79). In particular, we assume that for star forming galaxies the specific star formation rate, sSFR, evolves as $\text{sSFR} \sim 1/t$,

and that the probability of quenching depends predominantly on M_* . The different parameters in the calculations were derived by applying the continuity approach to the observed (evolving) stellar mass functions (see ref. (79) for details). These calculations predict that a galaxy with properties like those of CID–947 will evolve to reach $7.2 \times 10^{11} M_\odot$ at $z = 0$, if it *never* quenches. Alternatively, it can reach $2.2 \times 10^{11} M_\odot$ if it quenches at $z_{\text{quench}} = 2.51$, when the (mass-dependent) probability of quenching reaches 75%. Allowing for some additional mass growth through galaxy-galaxy mergers would increase the latter estimate of final mass by a factor of about 2.6, to $5.75 \times 10^{11} M_\odot$. The increase due to mergers for the former mass estimate is minute, since the probability of experiencing a similar-mass merger decreases with increasing mass. In any case, these calculations show that the stellar population in CID–947 should grow by about an order of magnitude between $z \simeq 3.3$ and $z \sim 0$.

We note that the high SFR we measure in CID–947 implies a molecular gas mass of at least $M(\text{H}_2) \simeq 2 \times 10^{10} M_\odot$, and perhaps as high as $2 \times 10^{11} M_\odot$ (80, 81). This suggests that the host galaxy can experience significant growth by consuming this reservoir of cold gas, without any additional gas accretion from its surroundings (i.e., the IGM), nor from mergers.

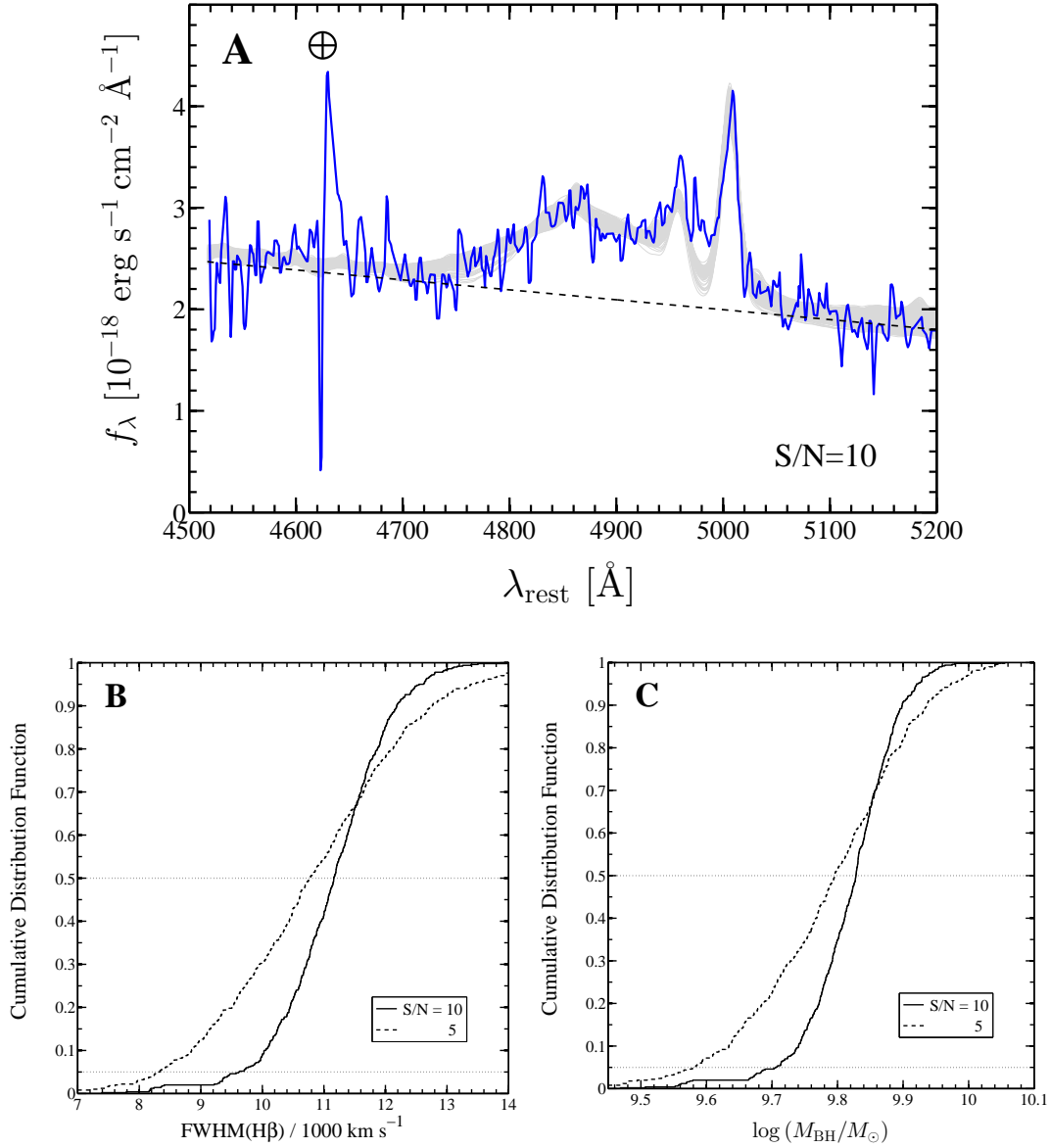


Figure S1: Results of the re-sampling simulations for the $\text{H}\beta$ emission complex of CID-947. *Top* - (A): Results for 500 simulations, with $S/N = 10$ and “nominal” $[\text{O III}]$ profiles (i.e., single-Gaussian). The diagram illustrates the original spectrum (blue), the best-fit linear continuum (dashed black), and the collection of 500 models that fit the simulated spectra (gray shaded region). *Bottom*: Cumulative distribution functions (CDFs) of the obtained line widths, $\text{FWHM}(\text{H}\beta)$ (B) and SMBH masses, M_{BH} (C). In both panels, the solid lines illustrate the results for the $S/N = 10$ simulation, while the dashed lines correspond to a more conservative simulation, with $S/N = 5$. The (dotted) horizontal lines mark the 5 and 50% (i.e., median) levels. We find that 95% of the $S/N = 10$ simulations resulted in $\text{FWHM}(\text{H}\beta) > 9615 \text{ km s}^{-1}$ and $M_{\text{BH}} > 5.09 \times 10^9 M_\odot$; and that 99% resulted in $\text{FWHM}(\text{H}\beta) > 8175 \text{ km s}^{-1}$ and $M_{\text{BH}} > 3.61 \times 10^9 M_\odot$.

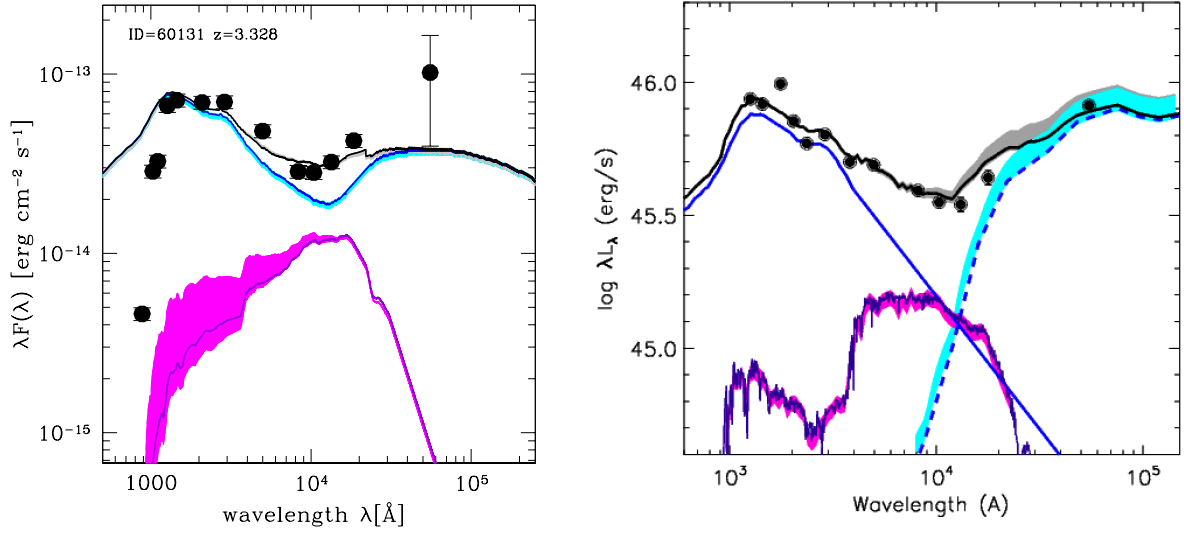


Figure S2: The UV-to-IR SED of CID-947, based on the available ground-based and *Spitzer* imaging data in the COSMOS field, which is used to infer the stellar mass of the host galaxy. *Left* - SED fitting from Bongiorno et al. (2012; (20)). The observed SED (black points) is fit by a model (black line) that consists of three distinct components: an un-obscured AGN, dominating the UV regime (solid blue) and a stellar population (magenta), which contributes a significant fraction of the emission around rest-frame wavelength of $\sim 1 \mu\text{m}$. *Right* - our own best-fitting model, in which the dusty toroidal structure, dominating the mid-IR regime (dashed blue), is treated separately from the intrinsic AGN emission.

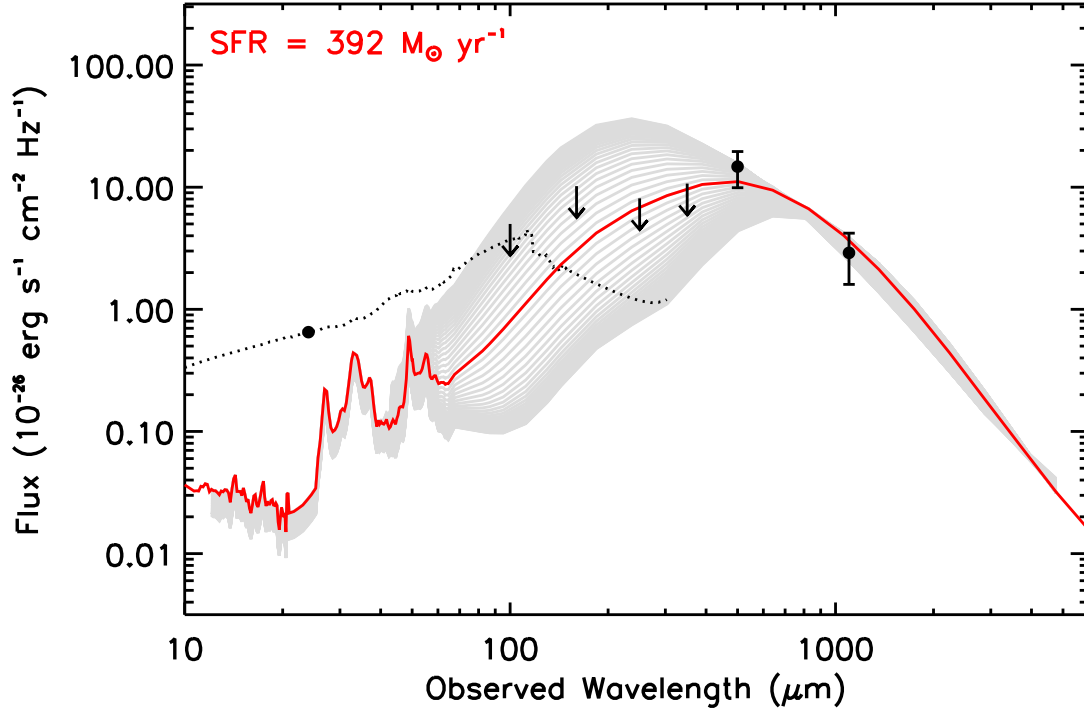


Figure S3: The mid-to-far IR SED of CID-947, based on the available *Spitzer* data and the low resolution *Herschel* and millimeter-wave observations, which is used to infer the star formation rate of the host galaxy. The gray lines represent a subset of the far-IR templates of star-forming galaxies we used (53), with the best-fit template and the corresponding SFR highlighted in red. The AGN contamination at sub-millimeter-to-millimeter wavelengths ($\lambda_{\text{rest}} > 200 \mu\text{m}$) is negligible, as illustrated by the pure-AGN spectral energy distribution (black dotted line; adapted from ref. (54)).

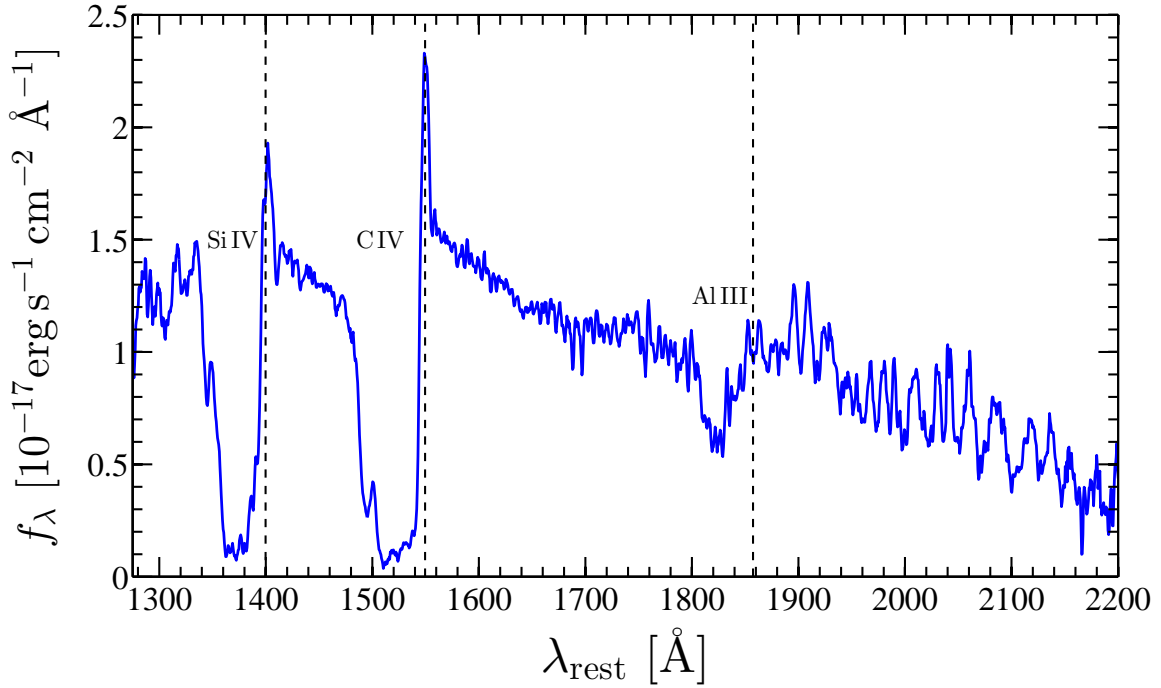


Figure S4: Optical spectrum of CID-947, probing the rest-frame UV regime, obtained as part of the zCOSMOS survey (70). Dashed vertical lines mark the expected center wavelength of the Si IV $\lambda 1400$, C IV $\lambda 1549$, and Al III $\lambda 1857$ lines. Blue-shifted, broad absorption features are clearly detected next to each of these three lines, identifying CID-947 as a low-ionization broad absorption line QSO (or “LoBAL QSO”). The broad absorption troughs blue-ward of Si IV and C IV reach $v_{\text{max}} \simeq 12000 \text{ km s}^{-1}$. The red part of the spectrum ($\lambda_{\text{rest}} \leq 1900 \text{ \AA}$), including the C III] $\lambda 1909$ line, is known to be affected by (instrumental) fringing.

Table S1: UV-to-IR Spectral Energy Distribution

Telescope/ Instrument	band	λ_{obs}	$m_{\text{AB}} \pm \Delta$	λ_{rest} [μm]	$\log(\lambda L_{\lambda}) \pm \Delta$ [erg s^{-1}]
Subaru/ SuprimeCam	V	5449 Å	20.900 ± 0.007	0.1259	45.937 ± 0.003
	r	6232 Å	20.803 ± 0.006	0.1440	45.918 ± 0.002
	i^+	7621 Å	20.394 ± 0.004	0.1761	45.994 ± 0.002
	z^{++}	8801 Å	20.588 ± 0.002	0.2033	45.854 ± 0.001
VISTA/ VIRCAM	Y	1.020 μm	20.639 ± 0.003	0.2357	45.770 ± 0.001
	J	1.250 μm	20.333 ± 0.003	0.2888	45.803 ± 0.001
	H	1.650 μm	20.290 ± 0.004	0.3813	45.700 ± 0.001
	K_s	2.154 μm	20.029 ± 0.005	0.4976	45.689 ± 0.002
<i>Spitzer</i> / IRAC	ch1	3.526 μm	19.734 ± 0.011	0.8147	45.593 ± 0.004
	ch2	4.461 μm	19.589 ± 0.009	1.0307	45.549 ± 0.003
	ch3	5.677 μm	19.349 ± 0.073	1.3117	45.540 ± 0.027
	ch4	7.704 μm	18.765 ± 0.075	1.7800	45.641 ± 0.028
MIPS	24 μ	23.68 μm	16.868 ± 0.026	5.4704	45.912 ± 0.010